Conformational distribution of poly(ethylene oxide) in molten phase and in aqueous solution by quasi-elastic and inelastic light scattering

1998 J. Phys.: Condens. Matter 10 10141

(http://iopscience.iop.org/0953-8984/10/45/004)

J. Phys.: Condens. Matter **10** (1998) 10141–10157. Printed in the UK PII: S0953-8984(98)93826-7

Conformational distribution of poly(ethylene oxide) in molten phase and in aqueous solution by quasi-elastic and inelastic light scattering

C Branca, S Magazù, G Maisano, P Migliardo and V Villari

Dipartimento di Fisica and INFM, Università di Messina, PO Box 55, Papardo, 98166 S Agata di Messina, Italy

Received 1 May 1998, in final form 29 July 1998

Abstract. We report on measurements performed by Raman scattering, PCS and ultrasonic velocity measurements on poly(ethylene oxide) both in the molten phase and in aqueous solution.

Increasing the polymerization degree, m, the Raman analysis of the D-LAM (disordered longitudinal acoustic mode) spectral contribution to the pure polymers reveals a behaviour of the centre frequency and linewidth which has been connected with an oligomer–polymer transition occurring at $m \cong 13$. In aqueous solutions the frequency increase towards values corresponding to the crystal ones and the sharpening of the D-LAM spectral contribution indicate that the addition of water destroys the intermolecular interactions and stiffens the coil structure. In addition evidence of a more ordered conformation with respect to the melt phase is presented.

The temperature analysis of the D-LAM band and of the hydrodynamic radius, evaluated by PCS, reveals that the solvent power of water increases up to $T = 45\,^{\circ}$C, decreasing at higher temperature.

Interpreted in conjunction with ultrasonic data, these apparently differing findings provide a coherent interpretative key capable of encompassing the structural properties of our systems.

Finally the role played by inter- and intra-molecular interactions is discussed within the framework of current theories.

1. Introduction

Recently poly(ethylene oxide) (PEO) has received growing attention not only from the applicative point of view. The simplicity of its structure and its unusual solubility in water [1, 2], in fact, make it a precious model system [3] for studying the interaction mechanisms of water with hydrophilic surfaces [4] and macromolecules.

The chemical structure, H–(O–CH_2–CH_2)$_m$–OH, of this synthetic polymer includes two terminal groups, H and OH, which play an important role in short compounds. The hydrophobic ethylene units and the hydrophilic oxygens, which alternate along the chain, are responsible for its amphoteric character [5]. The similarity of the ether oxygen spacing (2.88 Å) with that of the oxygens in water (2.85 Å) could explain the polymer solubility in water [5, 6], which persists in all proportions at temperatures lower than the boiling point of water [2]. Above this point it presents a miscibility gap that, by diminishing the polymerization degree, m, shifts towards greater temperatures and vanishes [7] for $m < 48$. PEO is commercially available in an extremely broad molecular weight (M_w) range. PEO with $m < 150$ is generally called poly(ethylene glycol), or for short PEG.

A wide variety of experimental techniques has been employed to investigate the conformation of PEO in the crystalline and molten state. In the isolated ethylene glycol

0953-8984/98/4510141+17$19.50

(EG) molecule, the basic entity of PEO, many equilibrium configurations can be obtained by rotation of the two CH_2OH groups around the C–C axis. IR, Raman and computer simulation studies [8] reveal, also in the liquid phase, the existence of an intra-molecular H-bond which makes the *gauche* conformation the most energetically favoured. In addition, the OH interacting groups promote links among adjacent chains [8], via hydrogen bonding, giving rise to many transient species. The findings so far agree with the conformational assignment for the crystalline state to internal rotation about the O–CH_2, CH_2–CH_2 and CH_2–O bonds of *trans–gauche–trans (tgt)* respectively. Crystalline PEO is retained to present a helical conformation that contains seven structural units CH_2–CH_2–O with two helical turns per fibre identity period (19.3 Å) [9, 10]. The structure of this polymer, in the melt or in solution, has continued to intrigue investigators over the years. Pursuit of understanding has led various theoretical studies to quite different results, while vibrational spectroscopy has been revealed to be difficult to apply with confidence, when a broad distribution of a large variety of conformations is involved. It has become clear, however, that a strongly disordered conformation is favoured in the molten state, while in aqueous solution the *tgt* conformation is stabilized, due to hydrogen bonds between the ether-oxygen chain and water molecules [7, 11].

The purpose of the present work is to show how the joint employment of Raman scattering, ultrasonic velocity measurements and photon correlation spectroscopy (PCS) can furnish complementary information on the structural length scales of PEO, both in the melt and in solution. The analyses of the Raman D-LAM (acronym for disordered longitudinal acoustic mode) spectral contribution, of PCS correlation functions and of adiabatic compressibility data afford the opportunity to characterize the dependence of the polymer structural parameters on polymerization degree, solvent content and temperature.

2. Experimental setup and sample preparation

We examined high purity samples, purchased from Aldrich-Chemie, of ethylene glycol (EG) and PEO with average M_w of 106, 200, 300, 400, 600, 900, 1000, 1540, 3400 Da and polydispersity factors, M_w/M_n, reported in table 1, both in melt and in aqueous solution at different concentrations. The wide range of commercially available M_w values makes PEO an ideal system for such a kind of study. The M_w average values and polydispersities were provided by the manufacturer. To investigate the role played by the interactive OH end groups, we also examined the CH_3 terminated species, corresponding to the same degree of polymerization of PEO. The solutions were freshly prepared and slowly filtered with 0.22 μm PTFE filters.

Polarized (I_{VV}) and depolarized (I_{VH}) spectra were obtained by a Spex Ramalog 5 triple monochromator in a 90° scattering geometry in the (−40 °C–80 °C) temperature range. To avoid fluorescence, which screens the Raman signal when short-wavelength laser excitations are used, the 5145 Å line of an argon laser was chosen. The laser power was maintained at approximately 5 W. The detection apparatus consisted of a photon counting system whose outputs were processed on line by a computer. The scattered photons were automatically normalized for the incoming beam intensity in order to ensure good data reproducibility. The optical purity of the samples ensured to collect data with good signal-to-noise ratio and with high reproducibility. The samples were sealed in optical quartz cells and then mounted in an optical thermostat which stabilizes temperature within ±0.1 °C.

The spectral range covered was −100–1600 cm^{-1}, with an instrumental resolution from 0.2 to 4 cm^{-1}, depending on the examined spectral range. The spectra at different resolutions were subsequently numerically matched and corrected for the density ρ, for the refractive

Table 1. PEOs polydispersity values.

M_w	$Q = M_w/M_n$
62	1.07
106	1.06
200	1.08
300	1.08
400	1.07
600	1.10
900	1.10
1000	1.09
1540	1.10
3400	1.10

index n and for local field effects. These corrections correspond to a normalization of the intensity by the factor $n\rho^{-1}(n^2+2)^{-4}$, with $n(T)$ and $\rho(T)$ taken from the literature. The spectral information which matters most in this study is the isotropic scattering intensities, calculated from the parallel and perpendicular components of the scattered light. In an ordinary (non-resonant) Raman effect, for linearly polarized excitations, the depolarization ratio $\rho = I_{VH}/I_{VV}$, which as well known varies in the range $0 \leqslant \rho \leqslant 3/4$, being nearly equal to 3/4 for fully depolarized bands, has been also evaluated.

The PCS measurements were performed using a photon counting optical system and a Brookhaven BI-30 correlator to analyse the scattered light. As exciting source, the 4880 Å vertically polarized line of a unimode argon laser, working in the power range of 50–400 mW, was used. The scattered light, by means of an optical fibre, was detected in a 90° scattering geometry. Samples, put in optical cells, were recirculated and filtered using a peristaltic pump and then mounted in an optical thermostat suitable built to avoid any unwanted stray-light contribution. Data collected for $M_w < 3400$ in the dilute region ($\phi < 0.15$) do not furnish reliable intensity autocorrelation functions. The measurements were performed in the $qR \ll 1$ region, where chain internal motions do not contribute.

Measurements of sound velocity, v, were performed by pulse echoes technique using a home-made thermoregulated ($\pm 0.01\,^{\circ}$C) acoustic interferometer working at a frequency of 3 MHz, purposely projected to assure accuracy of the velocity experimental measurements better than $\pm 0.1\%$. The electronic equipment consisted of a standard Matec Inc. apparatus and the measurements were performed using the echo overlapping method. Auxiliary measurements of density, ρ, necessary to evaluate the adiabatic compressibility through the relation $\beta = (\rho v^2)^{-1}$, were performed using the standard picnometer technique.

3. Raman and ultrasonic data

It is well known that the polarized and depolarized spectra measured in a Raman experiment are essentially connected with the Fourier transform of the polarizability tensor autocorrelation function:

$$J_{\nu\nu}(\boldsymbol{Q},t) \approx \langle \sum_{i,j,\nu,\nu'} (\varepsilon_s \tilde{\alpha}_I^{\nu}(0)\varepsilon_I)(\varepsilon_s \tilde{\alpha}_I^{\nu'}(t)\varepsilon_I) q_i^{\nu}(0) q_j^{\nu'}(t) \exp \mathrm{i}\boldsymbol{Q}[\boldsymbol{r}_i(t) - \boldsymbol{r}_j(0)] \rangle \tag{1}$$

where ε_s and ε_I are the scattered and incoming polarization vectors respectively, $\tilde{\alpha}^{\nu} = (\partial\tilde{\alpha}/\partial q)_{q=q_\nu}$, q_ν being the vibrational normal coordinate and $\boldsymbol{r}_i$ the position of the ith

scattering particle [12]. By polarization analysis, the different polarization character of the spectral contributions can be evidenced through the evaluation of the isotropic contribution:

$$I_{iso} = I_{VV} - 4/3 I_{VH}$$

The strongly polarised longitudinal acoustic mode (LAM) of polymers is commonly attributed to a complex of contributions representing the polymer skeletal bending and stretching vibrations [13]. According to the elastic rod model, which is appropriate for crystalline systems, the LAM frequencies are related to the stem length, l_K, undergoing the vibration, by the formula [14]:

$$\omega_{LAM} = kv = \frac{n}{l_K}\sqrt{\frac{E}{\rho}} \tag{2}$$

where n is an odd integer (for the selection rules we will be concerned with $n = 1$ since Raman activity is associated with a change in polarizability, and even values of n give no such change); E and ρ are the elastic modulus and density respectively. Although an approximation, relation (2) gives important information, in that the LAM frequency is inversely proportional to the rod length and directly proportional to the propagating velocity $v = \sqrt{E/\rho}$ of the longitudinal perturbation.

In non-crystalline systems the presence of conformational disorder dramatically changes the low-frequency Raman spectrum. The narrow LAM band, characteristic of the crystalline state, is replaced by the much broader polarized band associated with the disordered longitudinal acoustic mode (D-LAM) [15]. In such cases, l_K represents the length below which the coil can be treated as rigid (persistence length); it is essentially connected with the energy difference, $\Delta\varepsilon$, corresponding to the minima of the *trans–gauche* conformations [16, 17]. For the polyethylene chain, as well as for similar linear polymers, we have $l_K = l_0 \exp(\Delta\varepsilon/K_B T)$, where l_0 is of the order of a few ångströms. Increasing the ratio $\Delta\varepsilon/k_B T$, the percentage of *trans* conformations rises, namely the chain becomes locally less flexible [17]. The D-LAM spectra still depend on the statistical distribution of all-*trans* chain segments, but, in contrast with the $1/m$ dependence observed for the LAM modes of ordered chains, where m is the polymerization degree, a different experimental relation is found: $\omega_{D-LAM} = \omega_0 + B/m^2$, ω_0 and B being constants [18].

Figure 1 shows the Raman spectra, in the VV scattering configuration, of PEO 8000 in various phases. The arrows identify the D-LAM band. The spectral features of the molten state are greatly different from those of the solid phase. Specifically the helical splittings (1065 cm^{-1}) observed in the crystal disappear and frequency shifts are observed. These changes indicate a loss of order towards a far more disordered conformation.

The essential peculiarities of these spectra can be reproduced by superposing a series of normal coordinate calculations performed for an ensemble of conformers. Such a procedure, as recently reported by Yang *et al*, has led to the hypothesis, in the molten state, of an amount of *tgg* conformer greater than that predicted by previous simulation studies [19].

In aqueous solutions, instead, the Raman spectra are intermediate between the solid and the melt phase. The intensity of the ~ 811 cm^{-1} band of the solution sharply diminishes, while the ~ 1065 cm^{-1} band emerges from an unresolved contour. These findings indicate that PEO chains in aqueous solutions are more ordered with respect to the melt, assuming a considerable percentage of conformations similar to the *tgt* helix of the solid. The conformation ordering, which is further promoted by a lowering of temperature, can be associated with the hydration with environmental water molecules. On the other hand, the observation of a newly resolved band at ~ 918 cm^{-1} in aqueous solution, is demonstrative,

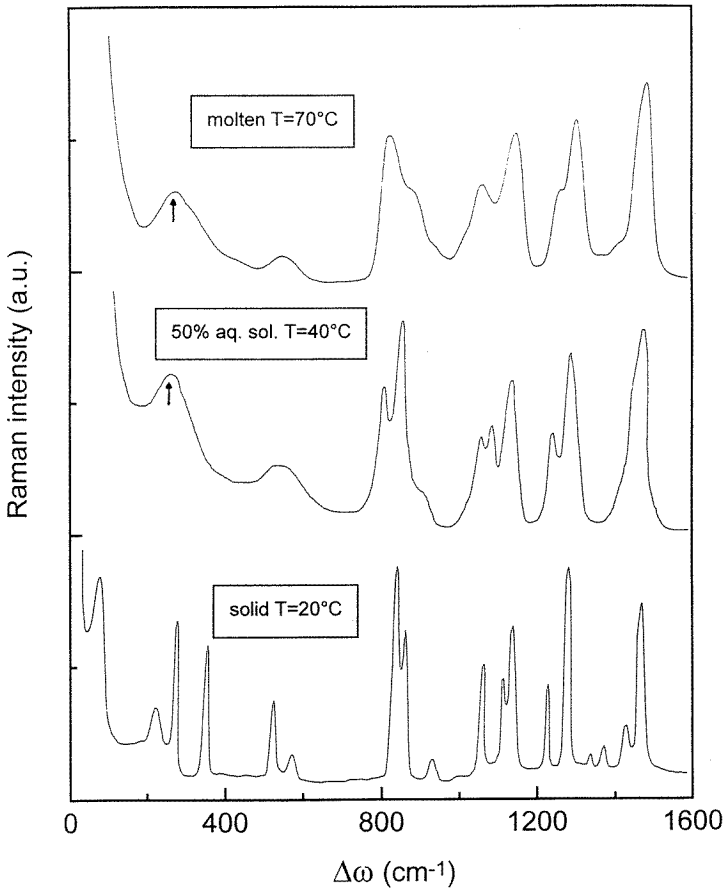

Figure 1. Polarized Raman spectra of PEO 8000 in different phases.

on the basis of the spectral assignment of [20] of the *gtgg* conformation for the OCH_2–CH_2–O–CH_2–CH_2O segment in aqueous solution, which possibly corresponds to the disordered part of the chain.

Figure 2 shows the I_{VH} spectrum for EG at $T = -40\,^{\circ}$C. The boson peak (BP) ($\omega_{BP} \approx 30$ cm^{-1}) and the D-LAM peak ($\omega_{D-LAM} \approx 340$ cm^{-1}) are clearly detected. The different polarization properties of the BP and of D-LAM emerge from the isotropic spectrum reported in the inset, which shows the D-LAM contribution whereas BP is absent, being completely depolarized. As illustrated by Torrell *et al* in a series of works [21, 22], BP is only weakly associated with intra-molecular modes; it rather reflects the collective dynamics governed by inter-chain interactions. The shape and position of BP, in contrast to D-LAM, is practically independent of the chain length. The comparison of the spectra obtained in EG and in the less interactive CH_3-terminated ethylene glycol dimethyl ether (EGDE) indicates a more marked BP contribution for EG, confirming that the resolution of the BP in *fragile* systems is less than in strong systems [23, 24]. So the role of the OH terminal groups, which determine an inter-chain connectivity, is evidenced [25, 26].

In figure 3 we present the isotropic Raman spectra relative to the D-LAM contribution for EG and PEO with average M_w of 106, 200, 300, 400, 600, 900, 1000 corresponding

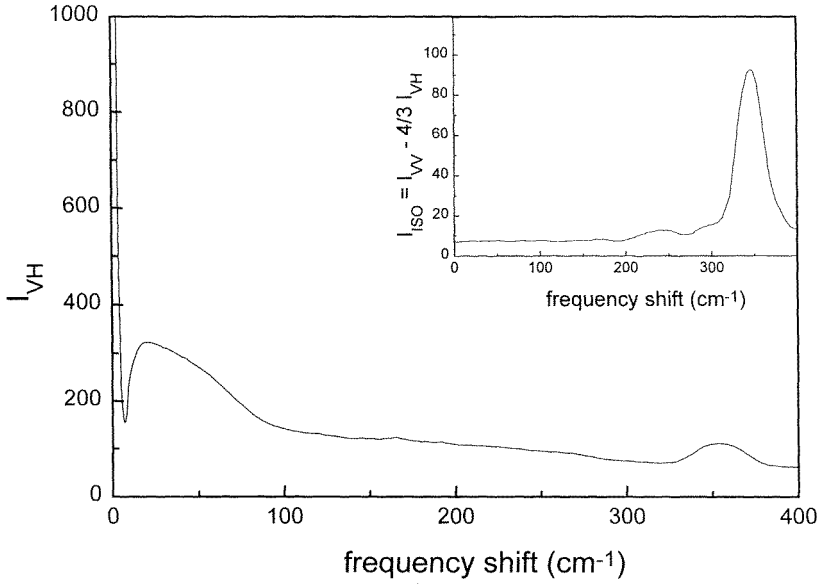

Figure 2. Depolarized Raman spectrum for EG at $T = -40\,^{\circ}$C. The isotropic contribution is reported in the inset.

to values of $m = 1$, 2, 4, 6, 9, 13, 20, 22 respectively. For $M_w = 106$ and 200, the bands turn into narrow, quite symmetric and well defined spectral contributions, due to the low disorder along few link chains. For increasing values of m, however, the bands shift towards low frequency and broaden; then they develop into a wide band for longer chains, assuming practically the same peak frequency and width for $m \approx 13$. A noteworthy result is obtained by the comparison, shown in figure 4, of the D-LAM contribution in EG and EGDE [27], where the active OH sites of EG are substituted by the non-interacting CH_3 groups. The noticeable centre frequency and width differences could be attributed to the different system compressibility and/or to the existence of intermolecular interactions among the EG molecules which give rise to a distribution of n-mers, with a greater spatial correlation length. To extract relevant information, we firstly tried different symmetric fitting functions. However, since, apart from the shortest chains, the spectra both in the pure compounds and in solution present strongly non-symmetrical profiles, we adopted a different fitting criterion. As pointed out above, the D-LAM contribution results from a non-homogeneous overlapping of sub-bands by the distribution of conformers existing in the liquid. So any substantial difference in the t–g distribution is reflected in the D-LAM band and can give rise to non-symmetric profiles [28, 29]. Therefore, instead of considering a multi-Gaussian fitting procedure, namely a number of distinct components related to different conformational structures, we consider it more appropriate to use a log-normal function which is extensively used for characterizing the chain length distribution of linear polymers, such are those we are dealing with:

$$I(\omega) = A \exp\left[-0.5\left(\frac{\ln(\omega/\omega_{D-LAM})}{\gamma_{D-LAM}}\right)^2\right] \tag{3}$$

where A is the amplitude, ω_{D-LAM} the band centre frequency and γ_{D-LAM} the *width* of the distribution. The characteristic frequency ω_{D-LAM} and width γ_{D-LAM}, obtained by the fitting procedure as a function of m, are reported in figure 5. As above indicated, both

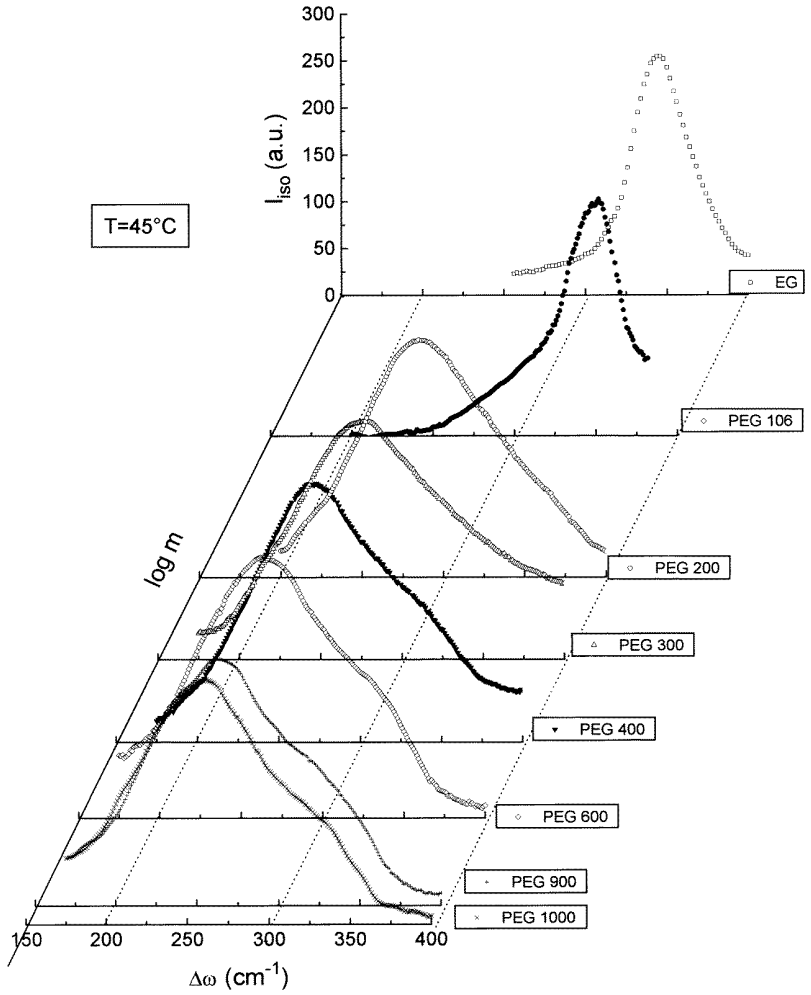

Figure 3. Isotropic spectra of the D-LAM contribution as a function of polymerization degree at $T = 45\,^{\circ}$C.

are strongly affected by the chain length in the low M_w range, whereas, by increasing m, a plateau value is reached above $m \approx 13$. The decrease of ω_{D-LAM} can be explained by taking into account that the (amenable to test) propagating velocity v of the disordered longitudinal acoustic mode within the coil is, in a sense, connected with the sound velocity measured in the system: $v = \sqrt{1}/\beta\rho$, β being the system adiabatic compressibility.

The $1/m^2$ dependence of the ultrasonic velocity, see figure 6, could justify the experimentally observed dependence of ω_{D-LAM} on the polymerization degree. On the other hand the trend of ω_{D-LAM}, γ_{D-LAM} and v is common to other physical quantities of the system, for example the polymer water interaction strength [5]. Taken together, these observations provide evidence for an oligomer–polymer transition for $M_w \geqslant 600$; this value, in a sense, defines the minimum length for which a polymer is *polymeric* in behaviour [25].

Now let us turn our attention to polymeric aqueous solutions. As figure 7 shows for PEG 600, by increasing the water content, the most striking features revealed in the D-LAM

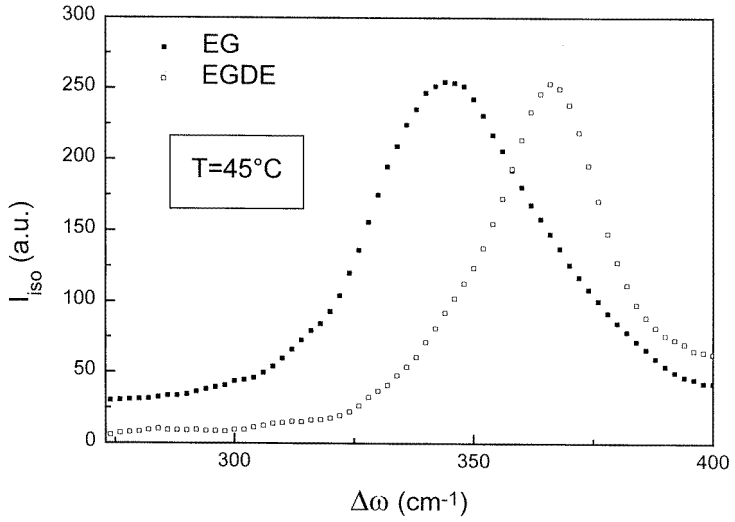

Figure 4. D-LAM contribution in ethylene glycol and in EGDE at $T = 45\,^{\circ}$C.

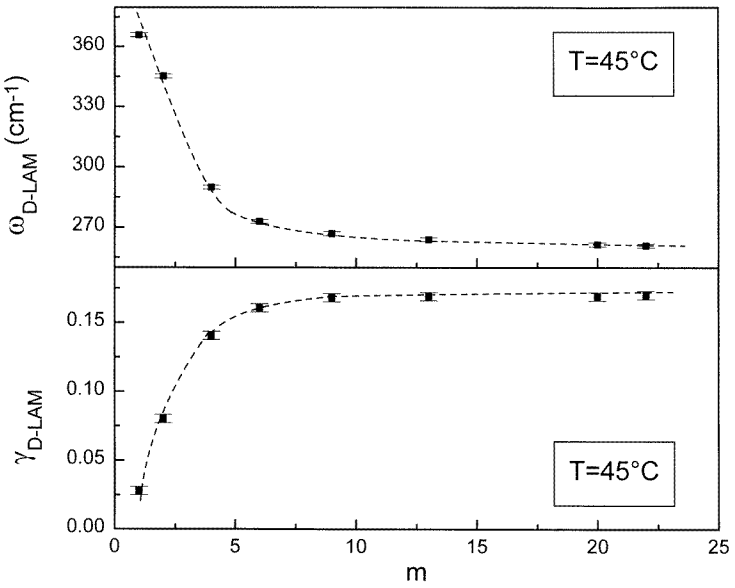

Figure 5. D-LAM centre frequency (ω_{D-LAM}) and width (γ_{D-LAM}) as a function of polymerization degree at $T = 45\,^{\circ}$C; the dashed lines are guides for the eye.

spectra are the remarkable frequency increase (over 10 cm^{-1}) towards values corresponding to the crystal ones, and the significative sharpening of the spectral contribution. Such evidence confirms that PEO in water tends to assume, in respect to the melt case, a more ordered conformation, closer to the crystalline one. The picture that emerges is that on adding water molecules, a certain number of these bond themselves, by H-bonds, to the oxygens of the oxirane groups, so promoting the formation of more rigid hydrated polymeric coils. This gives rise to the ω_{D-LAM} increase, and, on a macroscopic scale, to

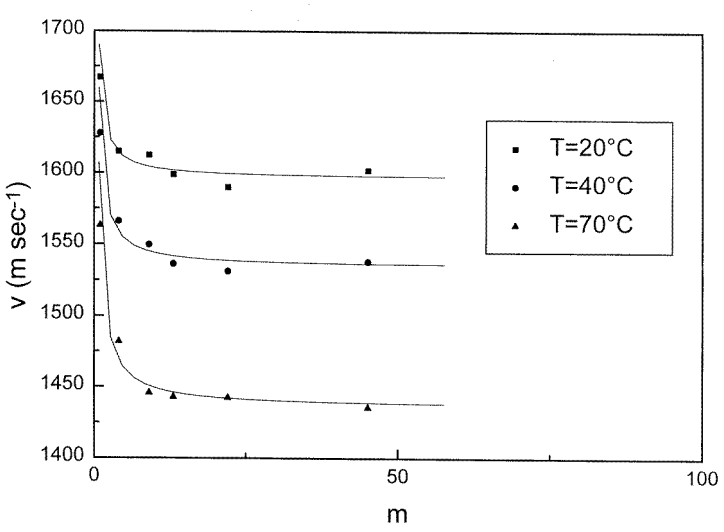

Figure 6. Ultrasonic velocity as a function of polymerization degree at three temperatures. The continuous lines are fit results.

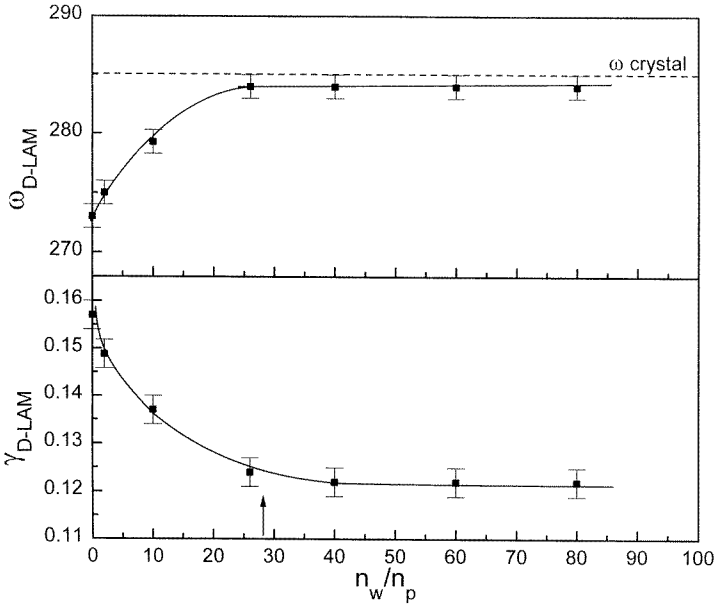

Figure 7. D-LAM centre frequency (ω_{D-LAM}) and width (γ_{D-LAM}) of PEG 600 aqueous solutions as a function of the water/polymer molar ratio; the continuous lines are guides for eye and the dashed line corresponds to the centre frequency of the band in the crystal. The arrow indicates the number of water molecules corresponding to a complete hydration shell of the PEG 600 molecule.

the diminishing of the system compressibility, see figure 8. It is plausible to hypothesize that the compressibility of the polymeric coil is closely connected with the compressibility of the entire system until a full hydration of the polymer chain is reached. A further

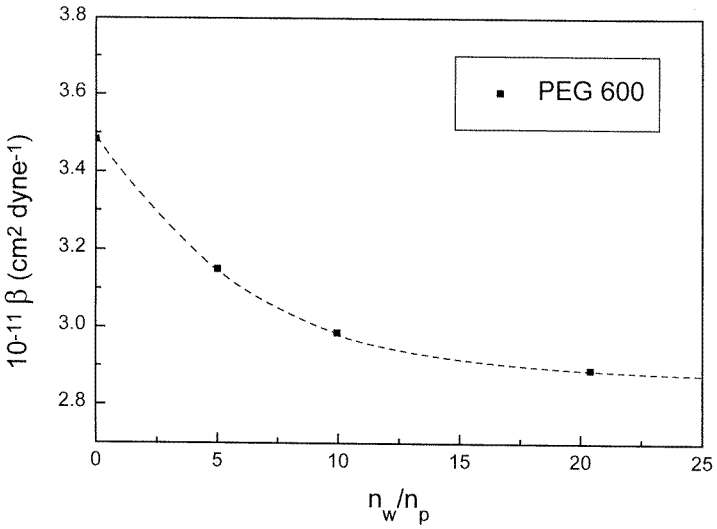

Figure 8. PEG 600 compressibility behaviour as a function of the water/polymer molar ratio; the dashed line is a guide for the eye.

addition of water molecules, in fact, introduces an amount of bulk water and, as a consequence, the measured system compressibility beyond the hydration values corresponds to the average value between that of the hydrated polymer and that of bulk water. This hydration process destroys the intermolecular interactions among the polymeric chains and promotes the sharpening of the D-LAM contribution, until, essentially, only one intense band, corresponding to the *isolated* hydrated polymer coil, is found. In this frame, as above stressed, the amount of water which signals the crossover to the ω_{D-LAM} and γ_{D-LAM} plateau values should correspond to the full hydration of the polymer.

To obtain information on the hydration number, we write the volume of the solution as: $V = n_p V_h + (n_w - n_p n_h)V_w$ where n_w and $_p$ are the water and the polymer molar number, n_h and V_h are the hydration number and the molar volume of the hydrated polymer and V_w the molar volume of the pure solvent. Differentiating with respect to pressure at constant entropy, under the hypothesis of the negligible compressibility of the hydrated polymer, we obtain for the hydration number:

$$n_h = \frac{n_w V_w \beta_w - V\beta}{n_p V_w \beta_w}. \tag{4}$$

Figure 9 reports for PEG 600 the hydration number as a function of temperature. The n_H behaviour is to be ascribed to the enhanced thermal motions that lead to lower residence times of water molecules in the nearby hydration of the polymer, in spite of the rupture of a certain fraction of hydrogen bonds in water which raises the number of water molecules available for bonding with the polymer. The hydration number value $n_h \approx 31$ at $T = 30\,^{\circ}\mathrm{C}$ is in excellent agreement with the crossover value for ω_{D-LAM} and γ_{D-LAM}. This result supports the interpretation, in terms of polymer hydration, of the ω_{D-LAM} and γ_{D-LAM} trend as a function of the water content.

Furthermore, the polymer hydration process gives rise to a temperature-dependent swelling process typical of a coil in a good solvent [17, 16]. Figure 10 shows, as an example, the temperature evolution of the D-LAM spectral contribution for PEO 3400 + 200 H_2O

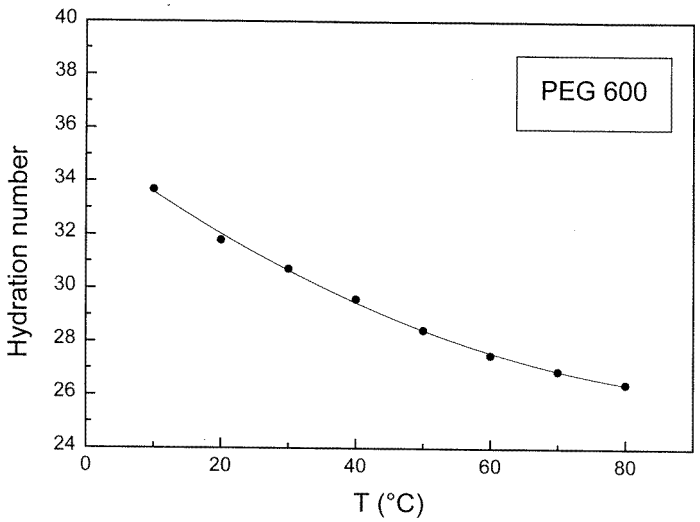

Figure 9. Hydration number for PEG 600 as a function of the temperature; the dashed line is a guide for the eye.

at three temperature values, $T = 10\,^{\circ}$C, $45\,^{\circ}$C and $60\,^{\circ}$C. The full lines running through the experimental points represent the fit result with equation (3). The chosen concentration value, assuring both a complete hydration of the polymer and a sufficient optical contrast for a good signal-to-noise ratio, corresponds to the plateau zones for ω_{D-LAM} and γ_{D-LAM}. As shown in figure 11, increasing temperature from 10 to $45\,^{\circ}$C, the salient features are a small frequency shift towards lower values and a significant broadening of the D-LAM mode. At higher temperatures, however, one observes an inversion in the behaviours of the ω_{D-LAM} and γ_{D-LAM} parameters. Such data indicate in the 10–$45\,^{\circ}$C range a broadening of the Kuhn length distribution towards higher values. The unusual behaviour can be accounted for in terms of the solvent power of water which increases for 20–$45\,^{\circ}$C, and then tends to decrease at higher temperature. As we shall see in the next section, these findings are in concordance with those obtained by PCS and with the behaviour of Mark–Houwink–Sakurada viscosity parameters [4], K and a, in the relation $\eta = KM_w^a$. In this latter case, which refers to a dilute solution of PEO, the marked variation of K and a with temperature from 10 to $35\,^{\circ}$C, see figure 12, demonstrates that water is becoming a markedly better solvent over this temperature range. The relatively much smaller variation from 35 to $45\,^{\circ}$C reflects the approach of its limiting value; finally, the water solvent power above $45\,^{\circ}$C begins to decrease with increase of temperature.

4. PCS data

The PCS experimentally measured quantity is the autocorrelation function of the scattered intensity, namely the second-order correlation function $G^{(2)}(t)$. Under the hypothesis of Gaussian statistics of the scattered field [30], satisfied in a dilute solution, $G^{(2)}(t)$ is related to the first order autocorrelation function $G^{(1)}(t)$ by the well known Siegert relation: $G^{(2)}(t) = 1 + |G^{(1)}(t)|^2$. Moreover for monodisperse spherical scatterers [31], $G^{(1)}(t)$ is simply exponential: $G^{(1)}(t) = \exp(-Dq^2)$ $q = (4\pi n/\lambda_0)\sin(\theta/2)$, D being the diffusion

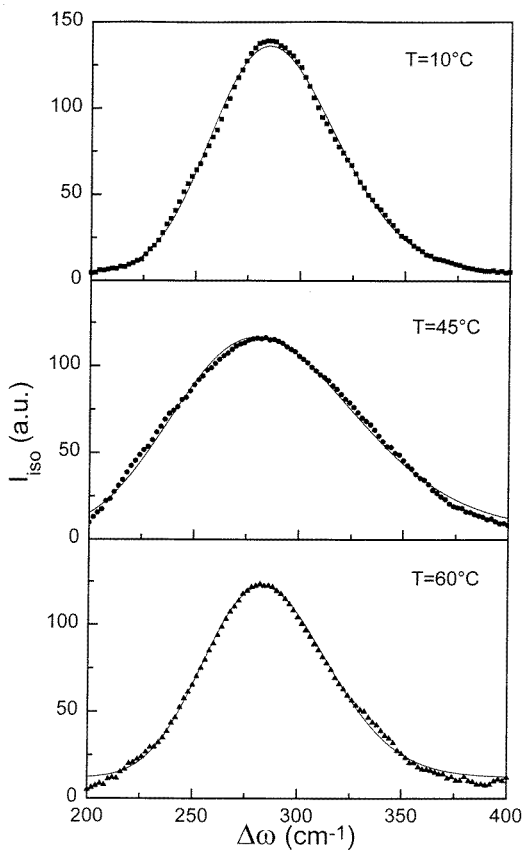

Figure 10. D-LAM contribution for a solution of PEO 3400 + 200 H_2O at different temperature values. The continuous lines represent the log-normal distribution (equation (3)).

coefficient, q the scattering wave-vector, n the solvent refractive index and λ_0 the incident wavelength. In the case of polydisperse solutions $G^{(1)}(t)$ becomes non-exponential because of the presence of a relaxation time distribution originated by the distribution of particle sizes [32]. Consequently, in such a case a standard cumulant analysis is more suitable:

$$\ln\left(c^{1/2}\left(\frac{G^{(2)}(t)}{A}-1\right)^{1/2}\right)=\ln c^{1/2}-\langle\Gamma\rangle(t)+\frac{\mu_2}{2}t^2-\frac{\mu_3}{6}t^3+\cdots \qquad (5)$$

where $\langle\Gamma\rangle$ is the first cumulant, related to the effective diffusion coefficient by [33] $\langle\Gamma\rangle = D_{eff}q^2$; μ_n is the nth moment of the distribution. In particular, for systems such as those we are dealing with, the second distribution moment, μ_2, is related to the polydispersity.

In the limit of infinite dilution D_{eff} tends to the free particle diffusion coefficient D_0. This latter, which is connected to the centre of mass motion of the isolated coil, allows us to determine the particle hydrodynamic radius by the Stokes–Einstein (SE) relation: $R_H = k_BT/6\eta\pi D_0$, where 6 indicates 'stick' conditions and η is the viscosity of water [30]. In figure 13, as an example, the D_{eff} behaviour as a function of volume fraction Φ is reported for PEO 3400 at three temperatures.

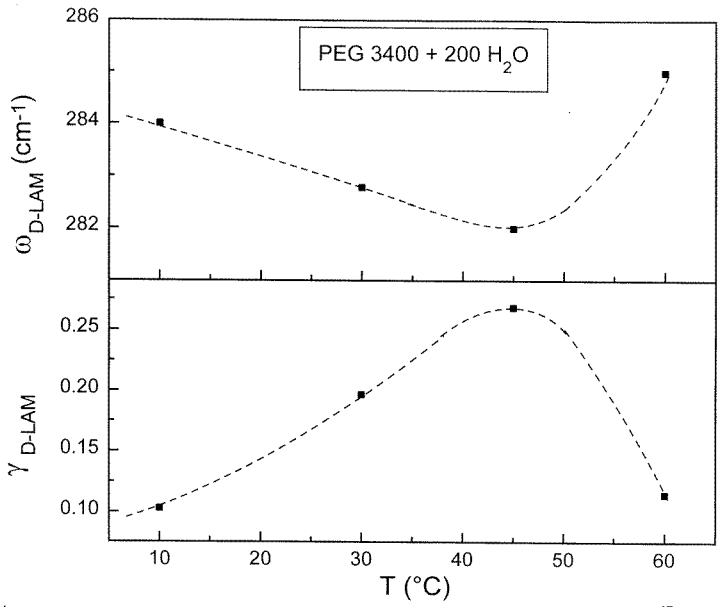

Figure 11. Temperature dependence of the D-LAM centre frequency (ω_{D-LAM}) and width (γ_{D-LAM}) for the aqueous solution of PEO 3400 + 200 H_2O. The dashed line are guides for the eye.

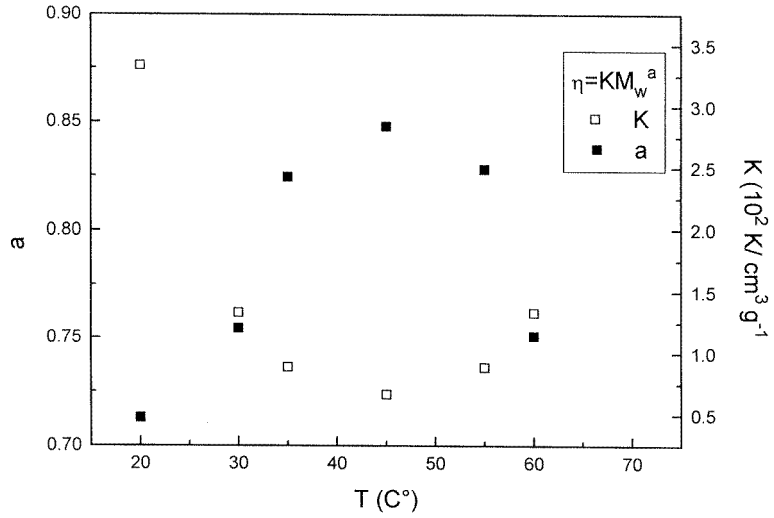

Figure 12. Behaviour of the Mark–Houwink coefficients, K and a, as function of temperature.

The concentration dependence of the diffusion coefficient can be examined through the Gibbs–Duhem expression as:

$$D_{eff} = \frac{k_B T}{\zeta_{ch}} \left(1 - \frac{N_A V_1}{M} \Phi\right) (1 + 2A_2 M \Phi)$$

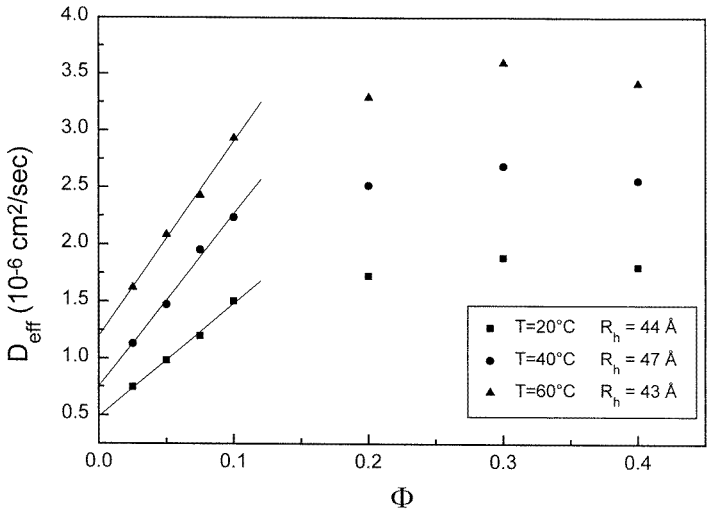

Figure 13. Effective diffusion coefficient behaviour as a function of volume fraction Φ. The continuous lines represent the fit result in the diluted regime by the linear law $D_{eff} = D_0(1 + K_D\Phi)$.

where ζ_{ch} is the frictional coefficient of the polymer molecule in solution, A_2 the second virial coefficient of the osmotic pressure, V_1 the partial specific volume of polymer with molecular weight M and N_A the Avogadro number. Therefore, the above cited concentration dependence involves chemical potential contribution, through the virial coefficient, and hydrodynamic interaction, included in the frictional coefficient. The concentration dependence of D_{eff}, however, is normally expressed by $D_{eff} = D_0(1+K_D\Phi)$ [34], where K_D, marking the initial slope of D_{eff}, depends both in sign and magnitude on the relative magnitudes of A_2 and ζ_{ch}. $K_D < 0$ indicates a *poor solvent* condition, namely a *collapsed* state intimately connected with the phase separation; $K_D = 0$ indicates a nearly *theta* condition (because at the *theta* temperature D_{eff} can be still dependent on concentration through the frictional coefficient), for which the effective interaction among the monomers vanishes; finally, $K_D > 0$ denotes a *good solvent* condition resulting from a 'repulsive' nature of the forces among the constituting monomers [35].

The initial increase of D_{eff} at low Φ clearly indicates a *swollen* state of the polymer coil. However, when Φ rises further D_{eff} goes towards a maximum indicating the transition towards a cooperative regime. Such a behaviour fulfills the general trend of D_{eff} obtained in polymeric solutions [36], colloidal suspensions [37] and by MD simulation [38].

The straight lines reported in figure 13 represent the fit result of D_{eff} against Φ in the dilute region, namely for $0 < \Phi < 0.1$, indicating that water behaves as a good solvent. In such a concentration region the polydispersity factor, evaluated using both water and methanol as solvent, is constant, revealing the absence of aggregative phenomena. The increase of K_D in the 20–40 °C temperature range and the successive saturation at higher temperatures supports the conclusions obtained from the D-LAM study, namely that the solvent power of water increases up to 45 °C and then decreases at higher temperatures.

From the extrapolated D_0 values, it is possible to evaluate the hydrodynamic radius by means of the SE relationship [30], $D_0 = k_BT/6\pi\eta R_H$. It is well known that the diffusing polymer and its hydrated shell are supposed to form a kinetic entity with respect

to translation, though the water molecules in the hydrated shell can change from time to time with those arriving from the farther environment [36]. In the case of PEO 3400, R_H increases from 44 to 47 Å in the temperature range 20–40 °C, and at higher temperatures decreases. This result can be explained by taking into account the competitive mechanisms between the increase of the repulsive intramolecular interactions, which swell the polymer structure [17, 16], and the decreasing of the hydration number with temperature, evidenced by ultrasonic velocity measurements (see figure 9).

Let us give a retrospective glance at the set of the collected data. Indicating with L the contour length of the polymer, and with N_K the number of constituting segments, the Kuhn segments being nearly independent, one has:

$$\langle R_H^2 \rangle = N_K l_K^2 = \left(\frac{L}{l_K}\right) l_K^2 = L l_K . \tag{6}$$

On the other hand, the temperature trend of the l_K values evaluated from PCS can be compared with the one obtained by Raman scattering, through the relationship:

$$l_K(T_2) = \frac{v(T_2)}{v(T_1)} \frac{\omega_{D-LAM}(T_1)}{\omega_{D-LAM}(T_2)} l_K(T_1) \tag{7}$$

where one takes as a reference value that obtained by PCS at the lowest temperature l_K (20 °C) = 16.7 Å. The similar trend of the l_K values obtained by PCS and Raman scattering, reported in figure 14, with a maximum at $T = 45$ °C, renders definitively convincing the interpretation of the temperature dependence of the polymer swelling process.

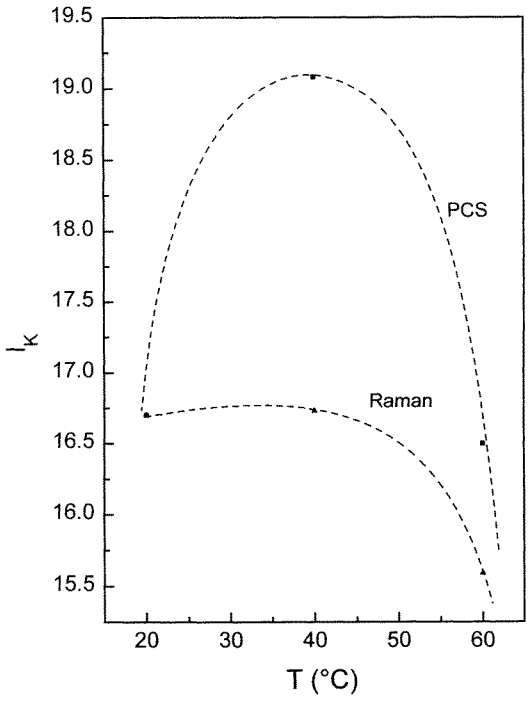

Figure 14. Temperature dependence of the Kuhn length, l_K, as obtained from PCS and Raman measurements. The dashed lines are guides for the eye.

5. Concluding remarks

The present work shows how the data obtained by Raman scattering, PCS and ultrasonic velocity measurements result in excellent agreement in characterizing the structural properties of polymeric systems.

As regards the pure samples, the D-LAM Raman analysis as a function of polymerization degree indicates the presence of an olygomer–polymer transition for $m \approx 13$. In contrast, the most striking features revealed in the D-LAM spectra in PEO aqueous solutions are the remarkable frequency increase towards values corresponding to the crystal ones, and the significative sharpening of the spectral contribution. These findings indicate that the addition of water destroys the intermolecular interactions and stiffens the coil structure, promoting a more ordered conformation in respect to that of the melt phase. Also in this frame it is possible to evidence a crossover of the ω_{D-LAM} and γ_{D-LAM} to plateau values in correspondence to a certain amount of water which signals the full hydration of the polymer. The evaluated hydration number, in excellent agreement with the crossover value for ω_{D-LAM} and γ_{D-LAM}, confirms the correctness of the interpretation. In aqueous solution, the temperature analyses of the Raman, PCS and ultrasonic data indicate clearly that the solvent power of water increases up to 45 °C and then decreases at higher temperatures.

In conclusion, in this paper we have sought to show how Raman, PCS and ultrasonic velocity measurements combine to provide detailed information on the conformational properties of polymeric systems. It is shown that, notwithstanding the fact that usually techniques as small angle neutron scattering (SANS) and PCS are employed for such kinds of study, also the joint employment of Raman and ultrasonic velocity measurements is able to furnish similar information.

Evidently much remains to be learned on the role played by the solvent in the structural properties of PEO and new experimental studies by SANS and NMR in different solvents are being performed to increase this knowledge.

References

[1] Kjellander R and Florin E 1981 *J. Chem. Soc. Faraday Trans.* **77** 2053
[2] Bailey F E and Callard R W 1959 *J. Appl. Polym. Sci.* **1** 56
[3] Barnes A C, Enderby J E, Breen J and Leyte J C 1987 *Chem. Phys. Lett.* **142** 404
[4] Molyneux P 1983 *Water-Soluble Synthetic Polymers: Properties and Uses* (Boca Raton, FL: Chemical Rubber Company)
[5] Magazù S 1996 *Physica* B **226** 92
[6] Bieze T W N, Barnes A C, Huige C J M, Enderby J E and Leyte J C 1994 *J. Phys. Chem.* **98** 6568
[7] Bailey F E and Koleske J V 1976 *Poly(Ethylene Oxide)* (New York: Academic)
[8] Crupi V, Jannelli M P, Magazù S, Maisano G, Majolino D, Migliardo P and Sirna D 1995 *Mol. Phys.* **84** 645
[9] Rabolt J F, Johnson K W and Zitter R N 1974 *J. Chem. Phys.* **61** 504
[10] Miyazawa T 1961 *J. Chem. Phys.* **35** 693
[11] Koenig J L and Angood A C 1970 *J. Polym. Sci.* A **8** 1787
[12] Volino F 1978 *Spectroscopic Methods for the Study of Local Dynamics in Polyatomic Fluids (NATO ASI-series B 33)* ed J Dupuy and A J Dianoux (New York: Plenum) pp 264–72
[13] Nishide H, Ohyanagi M, Okada O and Tsuchida E 1986 *Macromolecules* **19** 496
[14] Kim I and Krimm S 1996 *Macromolecules* **29** 7186
[15] Snyder R G and Strauss H L 1987 *J. Chem. Phys.* **87** 3779
[16] Grosberg A Y and Khokhlov A R 1997 *Giant Molecules* (New York: Academic)
[17] De Gennes P G 1979 *Scaling Concepts in Polymer Physics* (Ithaca, NY: Cornell University)
[18] Snyder R G 1982 *J. Chem. Phys.* **76** 3921
[19] Yang X, Su Z, Wu D, Hsu S L and Stidham H D 1997 *Macromolecules* **30** 3796

[20] Matsuura H and Fukuhara K 1985 *J. Mol. Struct.* **126** 251
[21] Ahlström P, Brodin A, Torell L M and Wahnström G 1998 *Phil. Mag.* B **77** 709
[22] Ahlström P, Wahnström G, Carlsson P, Schanz S, Brodin A, Maurer F and Torell L M 1998 *Phil. Mag.* B **77** 699
[23] Brodin A, Börjesson L, Engberg D, Sokolov A P and Torell L 1996 *Phys. Rev.* B **53** 11 511
[24] Sokolov A P, Kisliuk A, Quitmann D and Duval E 1993 *Phys. Rev.* B **48** 7692
[25] Börjesson L, Jacobsson P and Torell L M 1991 *J. Non-Cryst. Solids* **131–133** 104
[26] Wang C H, Lin Y H and Jones D R 1979 *Mol. Phys.* **37** 287
[27] A set of data for methyl-terminated PEOs at different molecular weight is reported in [25].
[28] Scherer J R and Snyder R G 1980 *J. Chem. Phys.* **72** 5798
[29] Snyder R G, Schlotter N E, Alamo R and Mandelkern L 1986 *Macromolecules* **19** 621
[30] Berne B J and Pecora R 1976 *Dynamic Light Scattering; with Application to Chemistry, Biology and Physics* (New York: Wiley)
[31] Cummins H Z and Swinney H L 1970 *Prog. Opt.* **8** 133
[32] Pusey P N 1974 *Macromolecular Diffusion in Photon Correlation and Light Beating Spectroscopy* ed H Z Cummins and E R Pike (New York: Plenum)
[33] Magazù S, Maisano G, Majolino D, Mallamace F and Micali N 1989 *Phys. Rev.* A **40** 2643
[34] Devanand K and Selser J C 1990 *Nature* **343** 739 and references therein
[35] De Gennes P G 1974 *J. Chem. Phys.* **60** 5030
[36] Schaefer D W and Han C C 1985 *Dynamic Light Scattering Applications of Photon Correlation Spectroscopy* ed R Pecora
[37] Segrè P N and Pusey P N 1996 *Phys. Rev. Lett.* **77** 771
[38] Klein R and Nägele G 1994 *Nuovo Cimento* **16** 963